



Published in final edited form as:

Proc IEEE Comput Soc Conf Comput Vis Pattern Recognit. 2008 ; : 1–8.

Localized Statistics for DW-MRI Fiber Bundle Segmentation

Shawn Lankton, John Melonakos, James Malcolm, Samuel Dambreville, and Allen Tannenbaum

Georgia Institute of Technology Atlanta, GA, USA 30322

Abstract

We describe a method for segmenting neural fiber bundles in diffusion-weighted magnetic resonance images (DWMRI). As these bundles traverse the brain to connect regions, their local orientation of diffusion changes drastically, hence a constant global model is inaccurate. We propose a method to compute localized statistics on orientation information and use it to drive a variational active contour segmentation that accurately models the non-homogeneous orientation information present along the bundle. Initialized from a single fiber path, the proposed method proceeds to capture the entire bundle. We demonstrate results using the technique to segment the cingulum bundle and describe several extensions making the technique applicable to a wide range of tissues.

1. Introduction

Segmenting an object from its background is a fundamental task in computer vision. A typical approach may be based on the assumption that the object and background have different statistical properties. This assumption has proven quite robust in many situations, but tends to fail when these statistics vary throughout a given region. The present work is based on the observation that in many real-world situations the statistical differences are only meaningful locally, not globally throughout a region. With this in mind, existing global approaches may be naturally extended to segment larger classes of images involving non-homogeneous regions.

In this note, we explore this property of locality in the active contour segmentation framework. Global regional models are typical in employing such an approach. For example, work by Chan and Vese, proposes separating the first moments of the intensity distributions [6]. More recently, Michailovich *et al.* demonstrate a method based on the Bhattacharyya distance for separating entire distributions [24]. In both of these cases, features from the entire interior and exterior are compared.

The key contribution of this work is successful application of the statistical localization approach to the segmentation of neural fiber bundles in diffusion weighted magnetic resonance imagery (DW-MRI). Specifically, we first demonstrate that methods involving global comparison of features tend to fail on such imagery. We then show that by extending these approaches to use statistics sampled locally, we can capture heterogeneous orientation information along fiber bundles. Figure 1 illustrates such local sampling regions. Once

initialized with a single fiber path in the bundle, the proposed method evolves an active surface driven by local statistics to capture the entire bundle as a single region.

We now briefly outline the remainder of this note. First, in Section 2, we provide a literature review and background of tractography and fiber bundle segmentation algorithms. Second, in Section 3, we describe our algorithm for locally constraining the region-based method. Next, in Section 4, we show results on the segmentation of the cingulum bundle using our full active surface implementation. Finally, in Section 5, we offer concluding remarks and provide an explanation of how these ideas and results may be extended to improve performance in future work.

2. Background

Since the advent of DW-MRI, a great deal of research has been devoted to finding and characterizing neural connections between brain structures. Image resolution is typically high enough that major white matter tracts, or bundles of densely packed axons, are several voxels in cross-sectional diameter [27]. The goal of tractography algorithms is to segment these fiber bundles from the DW-MRI datasets.

Early tractography methods were based on streamlines which employed local decision-making based on the principal eigenvector of diffusion tensors [26, 42, 4, 7]¹.

In these techniques, tracts are propagated from a starting point until they reach some termination criterion. Due to the local decision-making process, these methods have been shown to perform poorly in noise and often stop prematurely. These techniques also do not provide a measure of connectivity for the resulting tracts. Furthermore, several of these methods do not use the full tensor, reducing the data to the principal eigenvectors, and subsequently are unable to handle fiber crossings, branchings, “kissings,” etc.

Despite the shortcomings of this approach, streamlining has become the most popular method for fiber segmentation. To infer fiber bundles from streamline tractography results, several methods have been proposed for clustering fibers. The goal of clustering is to capture the behavior of a set of streamlines and to use this collective behavior to drive fiber bundle segmentation. The end result of clustering algorithms accurately captures many neural fiber bundles [28, 25].

Recently, another line of work has emerged which seeks to avoid the use of the problematic streamlines. Advances in tractography have been made which are able to find full brain optimal connectivity maps from predefined seed regions. These methods are more robust to noise, and depending upon the underlying metric, may be able to make use of the complete DW-MRI data rather than examining tensors. These approaches may be subdivided into stochastic and energy-minimization approaches.

Stochastic approaches produce probability maps of connectivity between a seed region and the rest of the brain. Parker *et al.* developed PICO, a probabilistic index for standard streamline techniques [32]. Perrin *et al.* presented probabilistic techniques for untangling fiber crossings using q-ball fields [34]. In other work, Friman *et al.* proposed a method for probabilistically growing fibers in a large number of random directions and inferring connectivity from the resulting percentages of connections between seed and target regions

¹The diffusion tensor is one of the simplest diffusion models. It is estimated from a set of diffusion weighted images, each probing the water diffusion in a different spatial direction. In the three-dimensional case the diffusion tensor is a 3×3 symmetric, positive definite tensor. For details see [5].

[9]. While providing a measure of connectivity between brain regions, these stochastic approaches do not provide an explicit segmentation of the fiber bundle itself and often do not explicitly provide the optimal connection between regions of the brain.

Energy-minimization techniques have also been developed. Parker *et al.* proposed fast marching tractography which minimizes an energy based on both the position and direction of the normal to a propagating front [33]. O'Donnell *et al.* cast the tractography problem in a geometric framework by finding geodesics on diffusion tensor manifolds [31]. Similarly, Prados *et al.* and Lenglet *et al.* demonstrated a Riemannian based technique, GCM (Geodesic Connectivity Mapping), for computing geodesics using a variant of Fast Marching adapted for directional flows [38, 18]. Jackowski *et al.* find geodesics using Fast Sweeping as given by Kao *et al.* [10, 13, 14]. Pichon *et al.* and Melonakos *et al.* use the more general Finsler metric to find optimal connections [35, 36, 23, 21]. Finally, Fletcher *et al.* demonstrated solving Hamilton-Jacobi-Bellman systems on the graphics processing unit to find geodesics in near real-time speeds [8]. In each of these methods, an optimal path is found which represents the best connection between the two regions under the given metric.

2.1. Prior Work

A number of surface evolution approaches have been described in the literature for fiber bundle segmentation which we briefly review. Rousson *et al.* [40] use a multivariate Gaussian distribution of the tensor components in a geodesic active region model to drive a surface evolution towards the segmentation of fiber bundles. The method is applied to the segmentation of the corpus callosum, but is unable to fully capture its curved character as discussed by the authors. In a follow-up paper [17] a similar segmentation framework in combination with a geodesic distance between tensors, and is shown to yield superior segmentation results especially, when segmenting curved fiber bundles. Rathi *et al.* [39] demonstrated modeling the entire tensor distribution to capture inhomogeneity, and Malcolm *et al.* [20] extended the technique to segmentation using graph cuts. Additionally, Awate *et al.* [3] segmented curved fiber bundles using Markov random fields.

Jonasson *et al.* proposed two different ways to address the segmentation of curved fiber bundles in a surface evolution setting: (i) a local approach [11], where the surface evolution speed is influenced by the similarity of a tensor in comparison to its interior neighbors, and (ii) a region-based approach, where the similarity measure is based on the notion of a most representative tensor within the segmented region [12]. In the latter case, capturing highly curved fiber bundles will be problematic because similarity is based on a single representative tensor. The approach proposed in this paper is similar to the work of [11] in as much as it uses local tensor similarities to drive the segmentation. However, Jonasson *et al.* use only a few adjacent pixels to determine local statistics. Our approach allows for entire local regions of pixels both inside and outside the evolving surface to compete thus making the technique more robust to noise and initialization.

The current work is also an extension of [22] where the authors perform segmentation of the cingulum bundle using a greedy flood-fill algorithm to find the tensor bundle from an initial anchor tract. In this previous work, an anatomical prior based on distance to the anchor tract was used to prevent leaks into surrounding structures. The current work uses a full level set segmentation framework and does not require such an anatomical prior to prevent leaks and successfully capture fiber bundles.

Finally, the proposed segmentation is based on that of [16] but has been extended to segment tensors. There have recently been other publications such as [37, 1, 19] demonstrating similar localized statistical segmentation schemes. These, are also able to

segment on heterogeneous structures, but have all been applied to structural MRI or natural images. This work is the first application of localized region based active contours to DW-MRI data to the best of our knowledge.

3. The Algorithm

An implicit assumption of classical region-based approaches (i.e., those which compare features across the full interior with features from the full exterior) is that the interior of the contour contains nearly homogeneous statistical features (in the sense as being able to distinguish interior and exterior statistically), such as mean intensity. Under this assumption, segmentation algorithms proceed by evolving the closed curve or surface to minimize an energy defined over these global features.

However, if features are heterogeneous across the entire interior or exterior of the object of interest, it becomes difficult to define a global region-based approach which will accurately segment the image. For instance, in the case of the cingulum bundle which curves strongly, the tensors across the bundle vary in orientation along the entire length, as shown in Figure 2. In this sagittal view, we see that it is difficult to define a feature on the space of tensors which uniquely separates the entire interior of the cingulum bundle from the exterior. However, we also notice that the tensor shape and anisotropy vary smoothly across the bundle. Hence, locally along the fiber one can define tensor features which are distinguishable from the exterior. In Figure 3 we illustrate this by examining the tensors globally as well as within a particular local region. Notice how examining local regions enables better statistical separation of interior and exterior regions.

We employ the key assumption that tensors in of the interior of the bundle will be statistically different from tensors in the exterior of the bundle if examined locally, as the basis of our technique. We re-formulate standard global statistical modeling techniques in terms of localized statistics to cope with the non-homogeneous nature of fiber bundles and the surrounding brain structures. We first describe the localized statistics and then show how they can be incorporated into a single energy functional to be minimized with a fully variational level set energy minimization framework.

3.1. Localized Statistics

Let \mathbf{T} denote a volume of tensors derived from a given DW-MRI volume and normalized such that $|\mathbf{T}(x)| = 1$ for every $\mathbf{T}(x)$ in the domain Ω_x . Also let S be a closed surface represented as the zero level set of a signed distance function ϕ i.e., $S = \{x | \phi(x) = 0\}$ [29, 30]. These representations are helpful in defining local statistics on the orientation of the tensors so that they can be easily incorporated into an active surface optimization model.

In order to describe localized statistics, we introduce a characteristic ball function in terms of a global radius parameter, r

$$\mathcal{B}(x, y) = \begin{cases} 1 & \|x - y\| < r \\ 0 & \text{otherwise.} \end{cases} \quad (1)$$

We use $\mathcal{B}(x, y)$ to mask local regions by setting r to be relatively small compared to the structure to be segmented. This function will be 1 when the point y is within a ball of radius r centered at x , and 0 otherwise. (Here, x and y represent independent spatial variables which each describe a 3D location in the volume.) This function is used in conjunction with the smoothed Heaviside function,

$$\mathcal{H}\phi(x) = \begin{cases} 1 & \phi(x) > -\epsilon \\ 0 & \phi(x) > \epsilon \\ \frac{1}{2} \left\{ 1 + \frac{\phi}{\epsilon} + \frac{1}{\pi} \sin\left(\frac{\pi\phi(x)}{\epsilon}\right) \right\} & \text{otherwise} \end{cases} \quad (2)$$

to select local interior and exterior regions. $\mathcal{H}\phi(y)$ therefore corresponds to the interior of the evolving front while $(1 - \mathcal{H}\phi(y))$ corresponds to the exterior. Furthermore, the local interior at point x is describes as the non-zero portion of $\mathcal{B}(x, y) \cdot \mathcal{H}\phi(y)$ while the non-zero portion of $\mathcal{B}(x, y) \cdot (1 - \mathcal{H}\phi(y))$ describes the local exterior at x . The interior and exterior regions are shown as (c) and (d) in Figure 1.

Tensors do not lie in a linear vector space, but instead on a conical manifold. In order to simplify tensor arithmetic, we use a log-Euclidean mapping to place these tensors in a linear vector space [2]. We may then use standard linear algebra to compute distances to calculate statistics such as the mean tensor. In this transformation we compute the matrix logarithm of the 3×3 positive definite symmetric tensor. The logarithm maps the tensors onto the log-Euclidean tangent plane where linear operations may be performed directly. The inverse mapping to return the conical manifold is a matrix exponential. Thus, in this space, the integral of a group of tensors, $\mathbf{T}(x)$ is computed simply as

$$\exp\left(\int_x \log(\mathbf{T}(x)) \, dx\right) \quad (3)$$

Thus, we define the local tensor interior and exterior means as

$$u(x) = \exp\left(\frac{\int_{\Omega_y} \mathcal{B}(x, y) \mathcal{H}\phi(y) \log(\mathbf{T}(y)) \, dy}{\int_{\Omega_y} \mathcal{B}(x, y) \mathcal{H}\phi(y) \, dy}\right), \quad (4)$$

and

$$v(x) = \exp\left(\frac{\int_{\Omega_y} \mathcal{B}(x, y) (1 - \mathcal{H}\phi(y)) \log(\mathbf{T}(y)) \, dy}{\int_{\Omega_y} \mathcal{B}(x, y) (1 - \mathcal{H}\phi(y)) \, dy}\right), \quad (5)$$

respectively. Finally, we define a log-Euclidean distance,

$$d_{LE}[\mathbf{T}_1, \mathbf{T}_2] = \|\log(\mathbf{T}_1) - \log(\mathbf{T}_2)\|^2, \quad (6)$$

using the standard L2 norm after the mapping.

3.2. Segmenting With Localized Statistics

With these well-defined localized statistics, we now introduce an energy functional with which we can evolve S in order to determine an optimal segmentation based on modeling local regions by $u(x)$ and $v(x)$. We define this energy in terms of the signed distance function, ϕ

$$E(\phi) = \int_{\Omega_x} \delta\phi(x) \int_{\Omega_y} \mathcal{B}(x, y) F(\mathbf{T}(y), \phi(y)) \, dy \, dx + \lambda \int_{\Omega_x} \delta\phi(x) \|\nabla\phi(x)\| \, dx. \quad (7)$$

where F is defined as

$$F = \mathcal{H}\phi(y) d_{LE} [\mathbf{T}(y), u(x)] + (1 - \mathcal{H}\phi(y)) d_{LE} [\mathbf{T}(y), v(x)]. \quad (8)$$

We then compute the gradient descent curvature flow that will minimize E using the calculus of variations. This reveals the following evolution equation:

$$\frac{\partial \phi}{\partial t}(x) = \delta \phi(x) \int_{\Omega_y} \mathcal{B}(x, y) (d_{LE} [\mathbf{T}(y), u(x)] - d_{LE} [\mathbf{T}(y), v(x)]) dy + \lambda \delta \phi(x) \operatorname{div} \left(\frac{\nabla \phi(x)}{|\nabla \phi(x)|} \right). \quad (9)$$

By evolving ϕ with this equation, we deform the surface S so that it moves from its initialization to an optimal segmentation of the fiber bundle. We employ the efficient level set implementation of [44] to obtain fast and accurate results from the level set evolution in three dimensions.

3.3. Initialization

The algorithm is initialized with a pre-computed anchor tract, representing the lowest cost path connecting two maximally spaced-out, pre-defined regions of interest on the fiber bundle to be segmented (in our case the cingulum bundle). This anchor tract is computed using the technique described in [21], but any similar tractography method could be substituted. The result is a single-pixel anchor tract that is then dilated using a $5 \times 5 \times 5$ ball-shaped structuring element. This produces an initial surface with definite interior and exterior regions.

4. Experiments

In this section we show experiments on the cingulum bundle. We first describe why the difficulty and medical importance of this particular structure make it a perfect example on which to demonstrate this technique. Next, we show the results of several experiments run on this structure that exemplify the favorable results obtained by this algorithm.

4.1. The Cingulum Bundle

Here, we motivate the problem of segmenting the cingulum bundle. The cingulum bundle is a 5-7 mm in diameter fiber bundle that interconnects all parts of the limbic system. It originates within the white matter of the temporal pole, and runs posterior and superior into the parietal lobe, then turns, forming a “ring-like belt” around the corpus callosum, into the frontal lobe, terminating anterior and inferior to the genu of the corpus callosum in the orbital-frontal cortex [41]. Moreover, the cingulum bundle consists of long, association fibers that directly connect temporal and frontal lobes, as well as shorter fibers radiating into their own gyri. The cingulum bundle also includes most afferent and efferent cortical connections of cingulate cortex, including those of prefrontal, parietal and temporal areas, and the thalamostriatae bundle. In addition, lesion studies document a variety of neurobehavioral deficits resulting from a lesion located in this area, including akinetic mutism, apathy, transient motor aphasia, emotional disturbances, attentional deficits, motor activation, and memory deficits. Because of its involvement in executive control and emotional processing, the cingulum bundle has been investigated in several clinical populations, including depression and schizophrenia. Previous studies, using diffusion tensor imagery, in schizophrenia, demonstrated decrease of fractional anisotropy in the anterior part of the cingulum bundle [15, 43], at the same time pointing to the technical limitations restricting these investigations from following the entire fiber tract.

4.2. Bundle Segmentation Results

We ran experiments on several datasets of DW-MRI volumes of normal brains. Each dataset contains seed and target points drawn by experts which were used to extract a single representative fiber within the bundle. From this initialization, we used the proposed technique to determine a surface which encloses the entire fiber bundle.

There is one major parameter used in this technique: the localization radius r that describes the formation of the localized statistics which drive the segmentation. This parameter was chosen based on anatomical knowledge that the diameter size of a tensor bundle is at most 7mm [41]. Hence, we used $r=7$ mm to ensure that the entire bundle would be included in statistical computations. The other parameter used in this technique is the weighting coefficient, λ in equation 7. This parameter determines the intrinsic smoothness of the surface. Because the surface is necessarily high in curvature due to its fine structure, we set this parameter at $\lambda = 0.001$. The values of λ and r were the only parameters used in the technique and were kept constant throughout all experiments.

Figure 4 shows the segmentation of the left cingulum bundle as well as the left and right cingulum bundles together. The initialization consists of a single fiber, and is shown as a thin white volume. The final segmentations are shown as thicker yellow volumes. Two views of the final segmentations are provided. Using the proposed method, the bundle is segmented without leaking, and captures the changing properties of the bundle as it bends around the corpus callosum. This is all accomplished without any explicit shape prior to defend against leaks. Furthermore, the smoothness of the detected tensor is ensured by the intrinsic properties of the evolving active surface.

5. Conclusion

This paper proposed a novel segmentation method for diffusion tensor images. The approach is based on a level-set segmentation technique separating localized tensor statistics. This fully variational surface evolution scheme is based upon a local mean modeling energy. The localization of the statistics allows it to capture directionally varying fiber bundles (specifically the cingulum bundle) simply but robustly. This is especially useful as many fiber bundles in the brain that curve strongly (e.g., the cingulum bundle, the arcuate fasciculus, the corpus callosum). Furthermore, the ability of local models to discriminate regions is able to prevent leakage without the need for shape or distance priors that in effect mask off unwanted parts of the segmentation.

Several other extensions are possible, such as the use of more sophisticated distance and similarity measures. The proposed localized method as well as global region-based segmentation methods will benefit from similarity metrics using the complete tensor information. In particular, more suitable tensor-based statistics may be explored in this framework, such as those employed by Lenglet *et al.* [17].

Acknowledgments

This work was supported in part by grants from NSF, AFOSR, ARO, MURI, MRI-HEL as well as by a grant from NIH (NAC P41 RR-13218) through Brigham and Women's Hospital. This work is part of the National Alliance for Medical Image Computing (NAMIC), funded by the National Institutes of Health through the NIH Roadmap for Medical Research, Grant U54 EB005149. Information on the National Centers for Biomedical Computing can be obtained from <http://nihroadmap.nih.gov/bioinformatics>.

References

1. An J, Rousson M, Xu C. γ -convergence approximation to piecewise smooth medical image segmentation. *Proc. Med. Imag. Comput. Comp. Assist. Interv.* 2007; 4792:495–502.
2. Arsigny V, Fillard P, Pennec X, Ayache N. Log-euclidean metrics for fast and simple calculus on diffusion tensors. *Magnetic Resonance in Medicine*. 2006; 56:411–421. [PubMed: 16788917]
3. Awate SP, Zhang H, Gee JC. A fuzzy, nonparametric segmentation framework for dti and mri analysis: With applications to dti-tract extraction. *IEEE Trans. Med. Imaging*. 2007; 26(11)
4. Basser P, Pajevic S, Pierpaoli C, Duda J, Aldroubi A. In vivo fiber tractography using DT-MRI data. *Magnetic Resonance in Medicine*. 2000; 44(4):625–632. [PubMed: 11025519]
5. Basser P, Pierpaoli C. Microstructural and physiological features of tissues elucidated by quantitative-diffusion-tensor MRI. *J Magn Reson B*. 1996; 111(3):209–219. [PubMed: 8661285]
6. Chan T, Vese L. Active contours without edges. *Image Processing, IEEE Transactions on*. 2001; 10(2):266–277.
7. Conturo T, Lori N, Cull T, Akbudak E, Snyder A, Shimony J, McKinstry R, Burton H, Raichle M. Tracking neuronal fiber pathways in the living human brain. *Proc Natl Acad Sci US A*. 1999; 96(18):10422–10427.
8. Fletcher T, Tao R, Jeong W, Whitaker R. A volumetric approach to quantifying region-to-region white matter connectivity in diffusion tensor MRI. *IPMI*. 2007
9. Friman O, Farnebäck G, Westin C. A Bayesian approach for stochastic white matter tractography. *IEEE Transactions on Medical Imaging*. 2006; 25(8):965. [PubMed: 16894991]
10. Jackowski M, Kao C, Qiu M, Constable R, Staib L. White matter tractography by anisotropic wavefront evolution and diffusion tensors imaging. *Medical Image Analysis*. 2005; 9:427–440. [PubMed: 16040268]
11. Jonasson L, Bresson X, Hagmann P, Cuisenaire O, Meuli R, Thiran J. White matter fiber tract segmentation in DT-MRI using geometric flows. *Medical Image Analysis*. 2005; 9(3):223–236. [PubMed: 15854843]
12. Jonasson L, Hagmann P, Pollo C, Bresson X, Wilson C, Meuli R, Thiran J. A level set method for segmentation of the thalamus and its nuclei in DT-MRI. *Signal Processing*. 2007; 87(2):309–321.
13. Kao C, Osher S, Qian J. Lax–Friedrichs sweeping scheme for static Hamilton–Jacobi equations. *Journal of Computational Physics*. 2004; 196(1):367–391.
14. Kao C, Osher S, Tsai Y. Fast sweeping methods for static Hamilton–Jacobi equations. *SIAM journal on numerical analysis*. 2005; 42(6):2612–2632.
15. Kubicki M, Westin C, Nestor P, Wible C, Frumin M, Maier S, Kikinis R, Jolesz F, McCarley R, Shenton M. Cingulate fasciculus integrity disruption in schizophrenia: a magnetic resonance diffusion tensor imaging study. *Biological Psychiatry*. 2003; 54(11):1171–1180. [PubMed: 14643084]
16. Lankton S, Nain D, Yezzi A, Tannenbaum A. Hybrid geodesic region-based curve evolutions for image segmentation. *Proc. SPIE: Med. Imag. Mar.2007* 6510:65104U.
17. Lenglet C, Rousson M, Deriche R. DTI segmentation by statistical surface evolution. *IEEE Transactions on Medical Imaging*. 2006; 25(6):685–700. [PubMed: 16768234]
18. Lenglet, C.; Rousson, M.; Deriche, R.; Faugeras, O.; Lehericy, S.; Ugurbil, K. A Riemannian Approach to Diffusion Tensor Images Segmentation.. *Proceedings of the 19th International Conference on Information Processing in Medical Imaging (IPMI)*; Glenwood Springs, CO, USA. 2005. p. 591-602.
19. Li C, Kao C-Y, Gore JC, Ding Z. Implicit active contours driven by local binary fitting energy. *Proc. Comput. Vis. Pattern Recog. Jun.2007*
20. Malcolm J, Rathi Y, Tannenbaum A. A graph cut approach to image segmentation in tensor space. *Workshop on Component Analysis Methods (CVPR)*. 2007
21. Melonakos J, Mohan V, Niethammer M, Smith K, Kubicki M, Tannenbaum A. Finsler tractography for white matter connectivity analysis of the cingulum bundle. *MICCAI*. 2007 to appear.

22. Melonakos J, Niethammer M, Mohan V, Kubicki M, Miller J, Tannenbaum A. Locally-constrained region-based methods for dw-mri segmentation. *Mathematical Methods in Biomedical Image Analysis (MMBIA)*. 2007
23. Melonakos J, Pichon E, Angenent S, Tannenbaum A. Finsler active contours. *IEEE Transactions on Pattern Analysis and Machine Intelligence*. 2007 in press.
24. Michailovich O, Rathi Y, Tannenbaum A. Image segmentation using active contours driven by the bhattacharyya gradient flow. *IEEE Trans. Image Process.* Nov; 2007 15(11):2787–2801. [PubMed: 17990755]
25. Moberts B, Vilanova A, van Wijk J. Evaluation of Fiber Clustering Methods for Diffusion Tensor Imaging. *Visualization, IEEE* 2005. 2005:9–9.
26. Mori S, Crain B, Chacko V, van Zijl P. Three-dimensional tracking of axonal projections in the brain by magnetic resonance imaging. *Ann Neurol*. 1999; 45(2):265–9. [PubMed: 9989633]
27. Mori S, van Zijl P. Fiber tracking: principles and strategies- a technical review. *NMR in Biomedicine*. 2002; 15(7-8):468–480. [PubMed: 12489096]
28. O'Donnell L. Cerebral white matter analysis using diffusion imaging. *Doctoral Thesis*. 2006
29. Osher, S.; Fedkiw, R. *Level Set Methods and Dynamic Implicit Surfaces*. Cambridge University Press; New York, NY: 2003.
30. Osher S, Tsai R. Level set methods and their applications in image science. *Commun. Math. Sci*. 2003; 1(4):1–20.
31. O'Donnell L, Haker S, Westin C. New Approaches to Estimation of White Matter Connectivity in Diffusion Tensor MRI: Elliptic PDEs and Geodesics in a Tensor-Warped Space. *Computing and Computer Assisted Intervention (LNCS)*. 2002; 2488:459–466.
32. Parker G, Haroon H, Wheeler-Kingshott C. A framework for a streamline-based probabilistic index of connectivity(PICo) using a structural interpretation of MRI diffusion measurements. *Journal of Magnetic Resonance Imaging*. 2003; 18(2):242–254. [PubMed: 12884338]
33. Parker G, Wheeler-Kingshott C, Barker G. Estimating distributed anatomical connectivity using fast marching-methods and diffusion tensor imaging. *Medical Imaging, IEEE Transactions on*. 2002; 21(5):505–512.
34. Perrin M, Poupon C, Cointepas Y, Rieul B, Golestani N, Pallier C, Riviere D, Constantinesco A, Le Bihan D. Fiber tracking in Q-ball fields using regularized particle trajectories. *Proc. of IPMI*. 2005; 2(3)
35. Pichon, E. PhD thesis. Georgia Institute of Technology; 2005. Novel methods for multidimensional image segmentation..
36. Pichon E, Westin C, Tannenbaum A. A Hamilton-Jacobi-Bellman approach to high angular resolution diffusion tractography. *Eighth International Conference on Medical Image Computing and Computer-Assisted Intervention (MICCAI05)*. *Lecture Notes in Computer Science*. 2005; 3749:180–187.
37. Piovano J, Rousson M, Papadopoulo T. Efficient segmentation of piecewise smooth images. *Proc. Scale Space and Var. Met. in Comp. Vis*. 2007; 4485:709–720.
38. Prados E, Lenglet C, Pons J, Wotawa N, Deriche R, Faugeras O, Soatto S. Control Theory and Fast Marching Techniques for Brain Connectivity Mapping. *Proceedings of the 2006 IEEE Computer Society Conference on Computer Vision and Pattern Recognition-Volume 1*. 2006:1076–1083.
39. Rathi Y, Michailovich O, Tannenbaum A. Segmenting images on the tensor manifold. *Computer Vision and Pattern Recognition*. 2007
40. Rousson M, Lenglet C, Deriche R. Level Set and Region Based Surface Propagation for Diffusion Tensor MRI Segmentation. *Computer Vision and Mathematical Methods in Medical and Biomedical Image Analysis*. 2004; 3(5):36.
41. Schmahmann, J.; Pandya, D. *Fiber Pathways of the Brain*. Oxford University Press; 2006.
42. Stieltjes B, Kaufmann W, van Zijl P, Fredericksen K, Pearlson G, Solaiyappan M, Mori S. Diffusion Tensor Imaging and Axonal Tracking in the Human Brainstem. *NeuroImage*. 2001; 14(3):723–735. [PubMed: 11506544]

43. Wang F, Sun Z, Cui L, Du X, Wang X, Zhang H, Cong Z, Hong N, Zhang D. Anterior Cingulum Abnormalities in Male Patients With Schizophrenia Determined Through Diffusion Tensor Imaging. 2004
44. Whitaker R. A level-set approach to 3D reconstruction from range data. *Int. J. of Computer Vision*. 1998; 29(3)

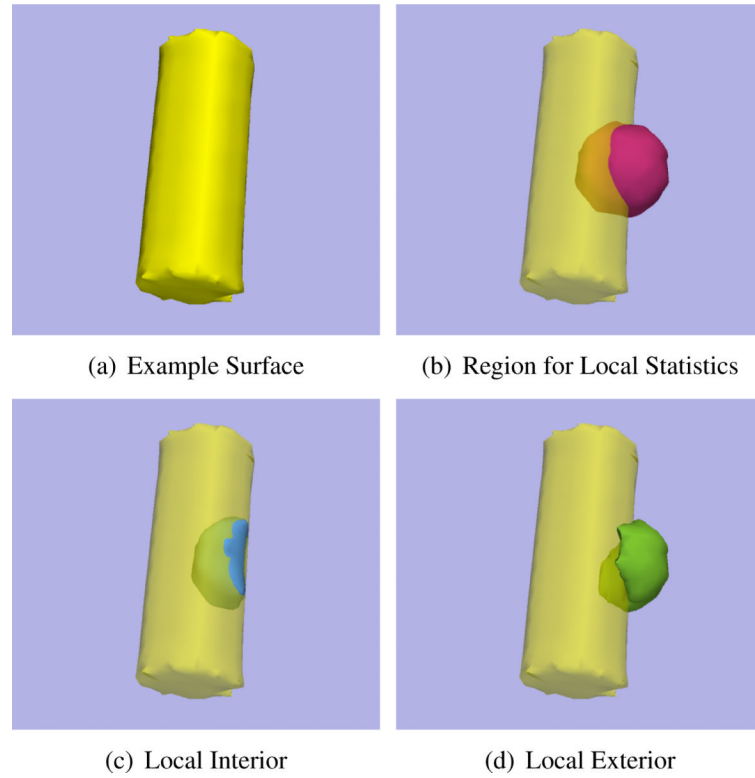


Figure 1. Visualization of the local regions over which tensor statistics are computed in order to segment fiber bundles with heterogeneous statistics.

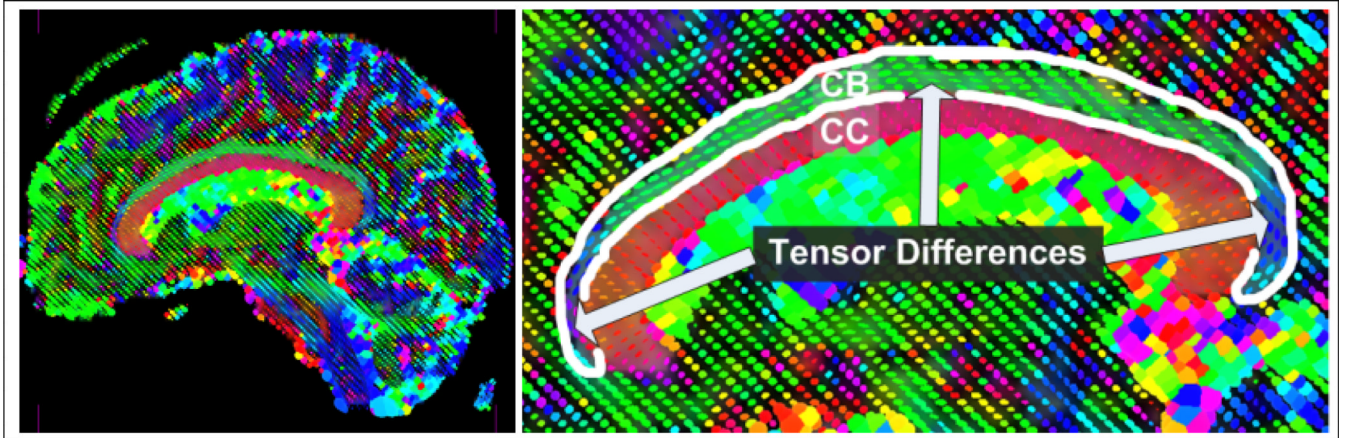
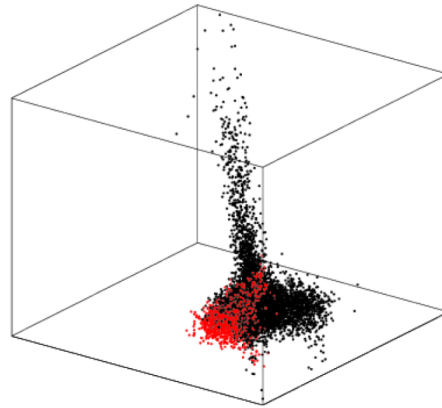
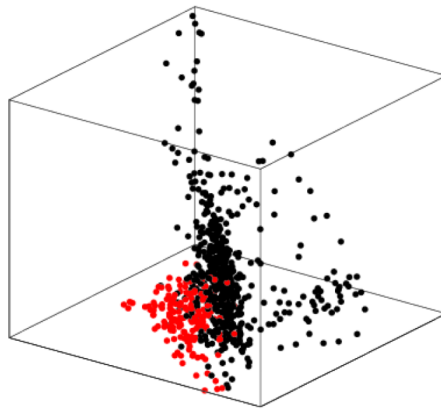


Figure 2.
Example of the need for local constraints on region-based segmentation algorithms which attempt to segment the cingulum bundle. Notice that tensor anisotropy and orientation vary across the length of the cingulum bundle.



(a) Interiors and exteriors using global statistics



(b) Interiors and exteriors using local statistics

Figure 3.

A visualization of the high-dimensional tensors in 3D by projection onto a unit vector. Tensors from the interior of the segmented fiber bundle are shown in *red*, and tensors from the exterior are shown in *black*. (a) Globally, interior and exterior tensors are mixed and not easily separable. (b) When a local region centered on a point on the surface of the fiber bundle is examined, interior and exterior tensors appear separable.

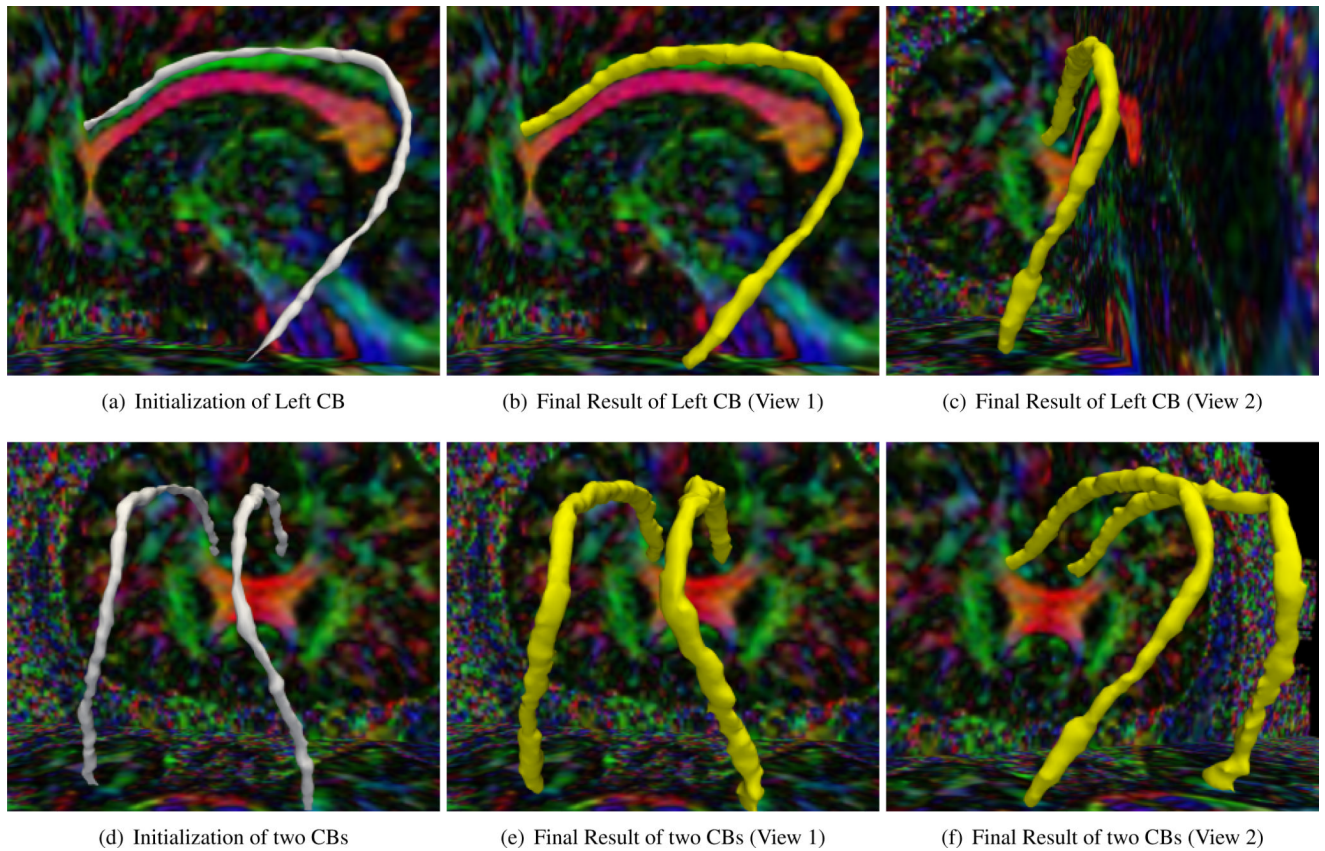


Figure 4.

Top Row: Segmentation of left cingulum bundle (CB). (a) Shows initialization from single anchor tract. (b,c) Show multiple views of the final segmentation. Bottom Row: Segmentation of left and right cingulum bundles (CBs) together. (d) Initialization from single tracts. (e,f) Multiple views of the final segmentation.